AIP | Review of Scientific Instruments

A source of high-power pulses of elliptically polarized ultrawideband radiation

Yu. A. Andreev, A. M. Efremov, V. I. Koshelev, B. M. Kovalchuk, A. A. Petkun, K. N. Sukhushin, and M. Yu. Zorkaltseva

Citation: Review of Scientific Instruments **85**, 104703 (2014); doi: 10.1063/1.4897167
View online: http://dx.doi.org/10.1063/1.4897167
View Table of Contents: http://scitation.aip.org/content/aip/journal/rsi/85/10?ver=pdfcov
Published by the AIP Publishing

A source of high-power pulses of elliptically polarized ultrawideband radiation

Yu. A. Andreev,[a] A. M. Efremov, V. I. Koshelev, B. M. Kovalchuk, A. A. Petkun, K. N. Sukhushin, and M. Yu. Zorkaltseva
Institute of High Current Electronics SB RAS, IHCE SB RAS, Tomsk 634055, Russia

(Received 27 June 2014; accepted 21 September 2014; published online 8 October 2014)

Here, we describe a source of high-power ultrawideband radiation with elliptical polarization. The source consisting of a monopolar pulse generator, a bipolar pulse former, and a helical antenna placed into a radioparent container may be used in tests for electromagnetic compatibility. In the source, the helical antenna with the number of turns $N = 4$ is excited with a high-voltage bipolar pulse. Preliminary, we examined helical antennas at a low-voltage source aiming to select an optimal N and to estimate a radiation center position and boundary of a far-field zone. Finally, characteristics of the source in the operating mode at a pulse repetition rate of 100 Hz are presented in the paper as well. Energy efficiency of the antenna is 0.75 at the axial ratio equal to 1.3. The effective potential of radiation of the source at the voltage amplitudes of the bipolar pulse generator equal to −175/+200 kV reaches 280 kV. © *2014 AIP Publishing LLC*. [http://dx.doi.org/10.1063/1.4897167]

I. INTRODUCTION

High-power sources of ultrawideband (UWB) radiation are widely used to study susceptibility of electronic systems to the electromagnetic pulse irradiation.[1] For this purpose, UWB sources with linear and elliptical polarization of electromagnetic field are developed. UWB sources with linear polarization are created using both single antennas and antenna arrays.

In high-power sources with a single antenna, such radiators as IRA,[2,3] TEM,[4,5] and combined antennas KA[6,7] are used. Antennas in UWB sources are excited with voltage pulses of different waveform including monopolar, bipolar, double-exponential as well as the damped radio-frequency ones.[8,9] By the present time, a line of high-power sources of UWB radiation has been developed based on the excitation of KA with bipolar voltage pulses of the length 0.2–3 ns at the pulse repetition rate of 100 Hz.[10–15] In all these sources a SINUS-160 voltage pulse generator was used. Pulse repetition rate is limited by the pulsed power supply of the SINUS-160 generator.

In high-power sources of UWB radiation with elliptical polarization of the field, the cylindrical helical antennas with a small number of turns find wide application.[16–18] Since a frequency range of 0.2–6 GHz is of interest for the investigations, then in Ref. 17 it is suggested to use a set of 9 helical antennas excited with a monopolar pulse of the amplitude >2 MB and length <2 ns at the pulse repetition rate of up to 100 Hz. Due to the limited frequency band, the helical antenna radiates a small part of energy from the electric pulse spectrum resulting in low energy efficiency of the radiation source.

To increase the efficiency of UWB radiation sources with elliptical polarization, it is suggested to excite helical antennas with bipolar voltage pulses of different pulse length. The first stage of the work is to create a source using a cylindrical helical antenna excited with a 1 ns bipolar voltage pulse. For numerical simulation of the radiator, a computer code[19] based on the finite-difference time-domain (FDTD) method has been developed.

Cylindrical helical antennas have been known for a long time and studied well.[20–23] Currently, the position of the radiation center and its stability in the frequency band of a short UWB pulse is debatable. Well-known studies using continuous waves[24–26] indicate that the phase center position depends on the frequency of radiation and diameter of a ground plate above which a helix is disposed. In this paper, the search of the radiation center is caused by the necessity of its estimation for measuring the antenna pattern.

II. SOURCE DESIGN

The source structure consists of the following main components presented in Fig. 1: a bipolar pulse generator consisting of a SINUS-160 monopolar pulse generator and a bipolar pulse former and a helical antenna in a dielectric container. The dielectric container was filled with SF_6-gas up to the gauge pressure of 0.8 atm. The source can operate both in a single pulse mode and at a pulse repetition rate of up to 100 Hz. The overall dimensions of the setup (excluding a support) are 260 × 70 × 40 cm.

III. A BIPOLAR PULSE GENERATOR

In a functional diagram of the bipolar voltage pulse generator shown in Fig. 2, a SINUS-160 monopolar pulse generator[6] is presented by an output forming line FL_0 and a switch S_0. This line could be charged from the secondary coil of the Tesla transformer up to the voltage of 360 kV with the pulse repetition rate of 100 Hz. The bipolar pulse former is assembled by the open-ended line circuit including the lines FL_1–FL_5, a sharpening S_1 and a cutoff S_2 switches, inductances L_1, L_2, a limiting resistor R_0, and a load R_L. At the S_0 switching, a charging voltage pulse arrived to the forming line FL_2 along the transmission line FL_1 through a limiting

[a]Electronic mail: andreev@lhfe.hcei.tsc.ru

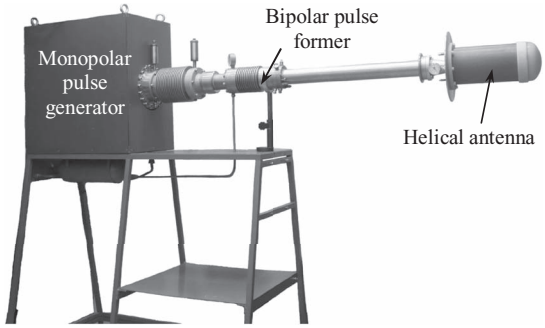

FIG. 1. A source of high-power pulses of elliptically polarized UWB radiation.

resistor $R_0 = 6\ \Omega$ and decoupling inductance L_1. When the charging voltage in the line FL_2 is close to maximum, the S_1 is switched on, and then, with a relative delay equal to double run along the line FL_3, the S_2 is switched on as well. In a 50 Ω transmission line FL_5, at the end of which a matched load R_L is installed, a bipolar voltage pulse is formed. The limiting resistor R_0 was used to decrease the bipolar voltage pulse oscillations in the FL_0–S_0–R_0–FL_1–L_1–FL_2–S_1–S_2 circuit, that extends the service life of the switch elecrodes. Inclusion of inductance $L_2 = 200$ nH at the end of the line FL_4 allows obtaining a more symmetrical waveform of a bipolar voltage pulse.[11]

Fig. 3 presents a design of a bipolar voltage pulse former. Inside the case, in the nitrogen medium under the pressure of 85 atm, three coaxial lines FL_2–FL_4, a sharpening S_1 and a cutoff S_2 switches, and inductances L_1, L_2 are placed. The line FL_4 has plexiglass insulation. Diameters of the internal conductors of the lines FL_2–FL_4 are equal to 35.6, 33, and 13.6 mm, respectively. Electrodes of the switch S_1 are the ends of the internal conductors of the lines FL_2, FL_3, and electrodes of the switch S_2 are a 2-mm-thick disk 1 and an insertion 2 at the case. All electrodes of the switches S_1 and S_2 are made of copper and installed with the gaps of 1.4 and 1 mm, respectively. A pulse of the charging voltage entered the line FL_2 from the SINUS-160 generator through the inductance L_1. A transmission line FL_5 with SF_6-gas insulation connects the output of the bipolar pulse former with either a resistive load or antenna (not shown in Fig. 3). An output bipolar voltage pulse was recorded by a TDS 6604 oscilloscope with the frequency band of 6 GHz through a coupled-line divider D_1 mounted inside the transmission line.

A bipolar pulse presented in Fig. 4 had the amplitudes of −175 and +200 kV and the length of 1 ns at the level of 0.1 of the amplitudes. During 1 h of operation of the generator at a pulse repetition rate of 100 Hz, the change in the voltage amplitude averaged by one hundred pulses (of both positive and negative half-waves) was not higher than 6%, and a root-mean-square deviation of the amplitudes σ during the same one hundred pulses was 3%–4%.

IV. HELICAL ANTENNA CHARACTERISTICS

Fig. 5(a) shows an external view of a cylindrical equidistant helical antenna. The helical antenna had the following parameters (Fig. 5(b)): the helix diameter $d = 85$ mm and the screen diameter $G = 300$ mm. A selected value d corresponded to the central frequency $f = 1.12$ GHz for the mode of axial radiation of the helical antenna, and this frequency was close to the maximum of the bipolar voltage pulse spectrum (1 GHz) of the length 1 ns entering the antenna input. The length of the helix along its axis L was determined by the number of turns N and the turn-to-turn distance $S = 60$ mm. In low-voltage test studies the number of the antenna turns varied from 5.5 to 3 with a step of 0.5 of the turn. To reduce the electric field strength and the wave impedance of the antenna, the turns of the helix were made of a thick copper tube of the diameter $a = 10$ mm. The wave impedance of the helix is close to the purely active one and for the central length of the radiation spectrum wavelength it can be estimated with the accuracy of up to 20% as

$$R = 140\left(\frac{C}{\lambda}\right),$$

where $C = \pi d$ is the circumference of the helical antenna.[27] The wave impedance of the antenna feeder is 50 Ω. To match the antenna to the feeder, the antenna part close to the input is not helical but parallel to a ground plate. The distance $h = 15$ mm between the ground plate and the conductor axis, forms a section with transforming impedance of 100 Ω.

Simulation of a voltage standing-wave ratio (VSWR) for helical antennas with various N was made using a 4NEC2 code.[28] According to the results of the simulations, the best matching of a helical antenna with a 50-Ω feeder in the region of low frequencies and near 1 GHz had the antenna with the number of turns $N = 4$. Measurements of helical antennas confirming the simulation results were carried out by an Agilent 8719ET Network Analyzer. Figure 6 presents the experimental and simulated VSWR for the antenna with $N = 4$. In addition, since the helical antenna was planned to be placed into the SF_6-gas atmosphere under the gauge pressure of 0.5–1 atm, the dielectric container influence on the antenna matching with the feeder was evaluated as well. The dielectric container with the wall thickness of 8 mm was made of polypropylene. The studies have shown that the above-mentioned container has insignificant influence on the antenna matching with the feeder. The lower boundary

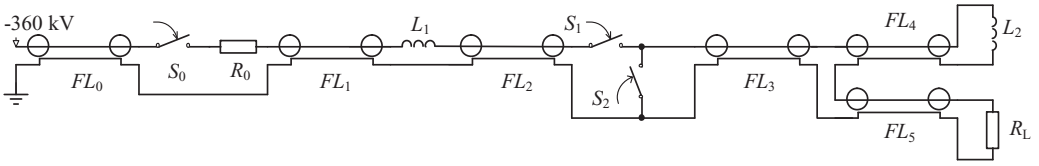

FIG. 2. Functional diagram of a bipolar pulse generator.

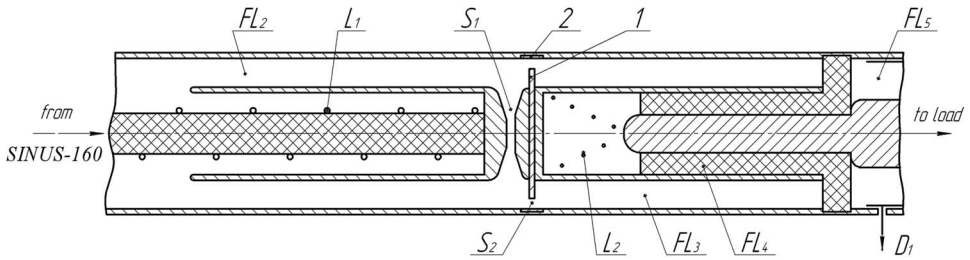

FIG. 3. Design of a bipolar pulse former. The former consists of FL_2–FL_4 coaxial lines, sharpening S_1 and cutoff S_2 switches, where 1 is the internal disk electrode and 2 is the external cylindrical electrode of S_2 switch, decoupling L_1 and pulse shape correction L_2 inductances and an output transmission line FL_5 with a coupled-line divider D_1.

frequency of the antenna matching band in the container slightly shifts towards the low-frequency region.

Measurements of radiation characteristics of the antennas were carried out in an anechoic chamber. The antennas were studied in the radiation mode. They were rotated in a horizontal plane. Bipolar voltage pulses with the duration of 1 ns were applied to the antenna inputs. To record the radiated pulses, a receiving antenna made as a half TEM-horn was used. The TEM antenna was chosen to measure patterns as making minimum distortions in the temporal pulse waveform of electromagnetic field. Depending on its orientation, the TEM antenna received either E_x or E_y components of electric field. To record the radiated pulses, a Tektronix TDS 6604 or a LeCroy Wave Master 830Zi-A oscilloscopes with the frequency band of 30 GHz were used. For helical antennas with $N = 3, 4, 5$ the waveforms of radiated pulses in the direction of the helix axis ($\theta = 0^\circ$) essentially differ from each other only at the end of the pulse. Peak values of the electric field strength vary slightly ($\leq$5%) towards reduction with decrease of the number of the helix turns N. Figure 7 presents comparative waveforms for the component E_y obtained in the direction $\theta = 0^\circ$ at a 3.2 m distance both in the experiment and FDTD code simulation, $N = 4$.

The radiated field was recorded at different distances. To reduce measurement errors of the helical antenna patterns, preliminary researches aimed to estimate the radiation center position of a helical antenna in the pulse excitation mode were carried out. The product of the peak field strength E_p by the distance r (at which the E_p was measured) vs. r was investigated.

Measurements were carried out along the antenna axis. To find the value $E_{p,}$ a receiving antenna made in the shape of two symmetric crossed dipoles was used.[29] This antenna has two outputs, each from its own dipole. Pulses corresponding to the dependence of the electric field components E_x and E_y on time were applied simultaneously to the different inputs of the LeCroy Wave Master 830Zi-A oscilloscope. In accordance with these components, a hodograph of vector $\boldsymbol{E}$ was plotted and the E_p value was found. In the studies of the value $rE_p(r)$, the bipolar voltage pulses of the amplitude $\pm$36 V and duration 1 ns were applied to the antenna input.

Compactness of the receiving antenna (the length of the symmetric dipoles was 4.7 cm) allowed measuring a pulsed field inside the helix at a removed dielectric container. Minimum distance from the ground plane (GP) to the receiving antenna was 6 cm. Figure 8 presents the measurement results.

In the far-field, the pulse amplitude decreases proportionally to $1/r$. Therefore, the boundary of the far-field zone is the distance from the radiation center r_f starting from which the product rE_p is a constant value.[7] Having measured the dependence $E_p(r)$, one can plot various dependences $rE_p(r)$ differing by a reference point r. Curve 1 in Fig. 8 corresponds to the reference case $r = 0$ at the GP. The dependence $rE_p(r)$

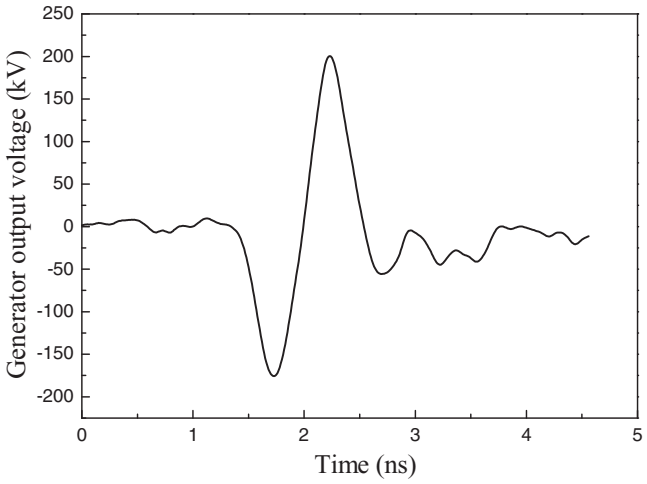

FIG. 4. Generator output bipolar voltage pulse.

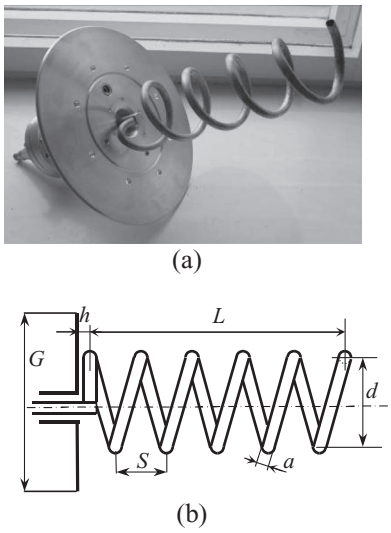

FIG. 5. External view (a) and geometry (b) of helical antenna: $G = 300$ mm, $S = 60$ mm, $d = 85$ mm, $a = 10$ mm, $h = 15$ mm, and $L = NS$ ($N = 3, 3.5, 4 \ldots 5.5$).

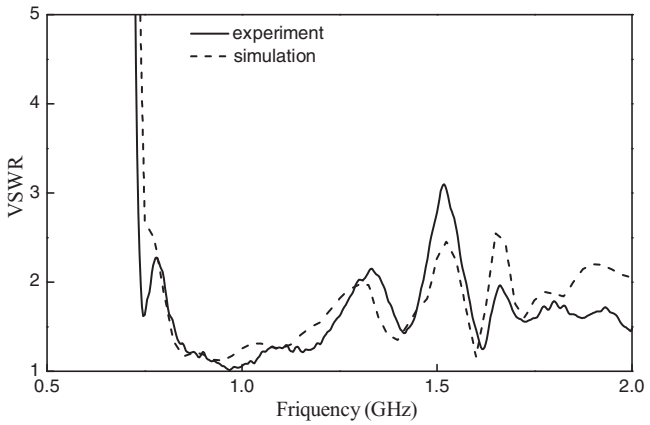

FIG. 6. Experimental and calculated dependencies of VSWR for helical antennas with $N = 4$.

increases sharply and then decreases gradually approaching asymptotically from above to the constant value. If the reference point ($r = 0$) is the end of the helix (the distance equal to $L + h$ from the GP), then the corresponding dependence will increase gradually up from below to a constant value (curve 2, Fig. 8). For convenience, the distance r in Figure 8 is adjusted so that the reference point for all the curves is the GP. We will consider that the radiation center of the antenna is a point at its axis which, being taken as a reference point, allows obtaining minimum distance from the boundary where $rE_p \cong$ const. In our case $r_f \cong 48$ cm ($r_f \cong 60$ cm from the GP). Meanwhile, the antenna radiation center corresponds to the region near the antenna axis at a distance L_c from the GP equal to $L_c = ((L + h)/2) - 1.5 \cong 11$ cm or in the wavelength $L_c/\lambda = 0.38$ (for $\lambda = 30$ cm). Dependence $rE_p(r)$ plotted for the reference case $r = L_c = 0$ is presented in Fig. 8, curve 3. To estimate the dependence of the radiation center position on the angle θ, the analogous measurements ($\theta = 0^\circ$) were made for $\theta = \pm 30^\circ$. The studies have shown that the radiation center is inside the helical antenna, but its position depends on the observation angle. For the chosen observation angles, the radiation center position corresponds to $L_c \cong 18$ cm ($L_c/\lambda = 0.6$) and is shifted relative to the axis by $\Delta r = \pm 3$ cm ($\Delta r/\lambda = 0.1$).

When measuring the pattern, the antenna was rotated around the axis passing through the point corresponding to the radiation center position at $\theta = 0^\circ$. If antenna was placed into the dielectric container, we considered that the radiation center position was not varied.

The position of the far-field zone boundary of the cylindrical helical antenna will be estimated as a distance beginning from which the hodograph $\boldsymbol{E}$ has no changes in the shape or inclination for the chosen observation angles θ and φ. Meanwhile, the condition $rE_p \cong$ const. is fulfilled as well. For this purpose, simulations and measurements of the vector $\boldsymbol{E}$ hodograph were carried out for various distances along the antenna axis and directions $\theta = \pm 30^\circ$ for arbitrary φ. Fig. 9 shows simulated and measured hodographs of $\boldsymbol{E}$ along the axis of the helical antenna at the 33 and 122 cm distances from the GP.

The axial ratio (AR) is seen to be decreased with the distance. For $\theta = 0^\circ$ and $\theta = \pm 30^\circ$, the experimental and simulated dependencies of the AR value on the distance r were obtained (Fig. 10), where the GP antenna position corresponds to $r = 0$. The above-mentioned dependence is plotted in Fig. 10 for the observation angle $\theta = 30^\circ$. The dependence for the observation angle $\theta = -30^\circ$ is analogous. From the results obtained, it follows that $r \cong 1.2$ m corresponds to the far-field zone boundary. All subsequent measurements were made in the far-field zone.

Boundary frequencies of the radiated pulse spectra by the level of -10 dB correspond to 0.68 and 1.45 GHz, respectively. Note, that for 1.0 GHz $< f <$ 1.45 GHz frequency band, where the condition $D > \lambda$ is fulfilled, the value of the far-field zone boundary is determined as[27]

$$r = \frac{2D^2}{\lambda},$$

where $D = G$ and λ is the radiation wavelength corresponding to the frequency f. For this frequency band, maximum value of the distance r is 0.87 m. For the lower frequency band of 0.68 GHz $< f <$ 1.0 GHz, the value $D < \lambda$ and the far-field zone is determined by the expression $kr \gg 1$, where $k = 2\pi/\lambda$. This expression can be written as $r \gg \lambda/2\pi$. Multiplying the

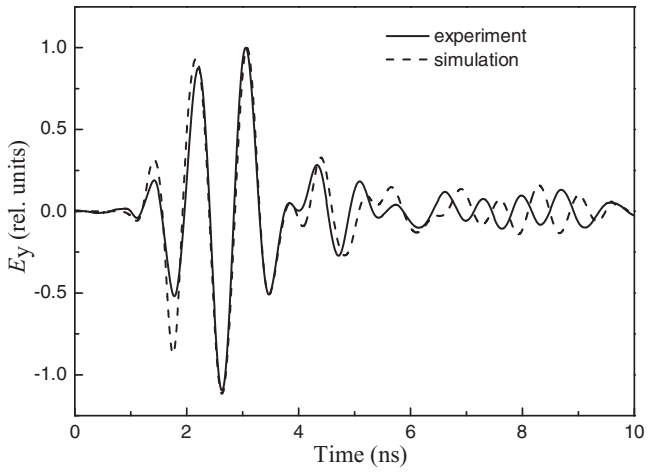

FIG. 7. Experimental and simulated waveforms of radiation in the direction of helix axis ($\theta = 0^\circ$) for antenna with $N = 4$.

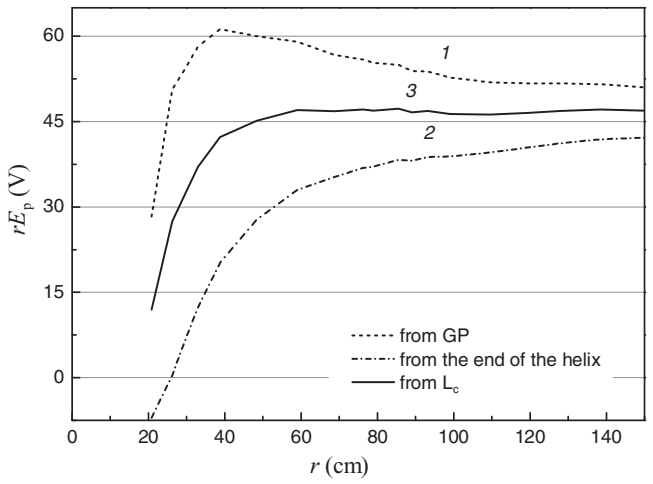

FIG. 8. Dependence of rE_p on the distance.

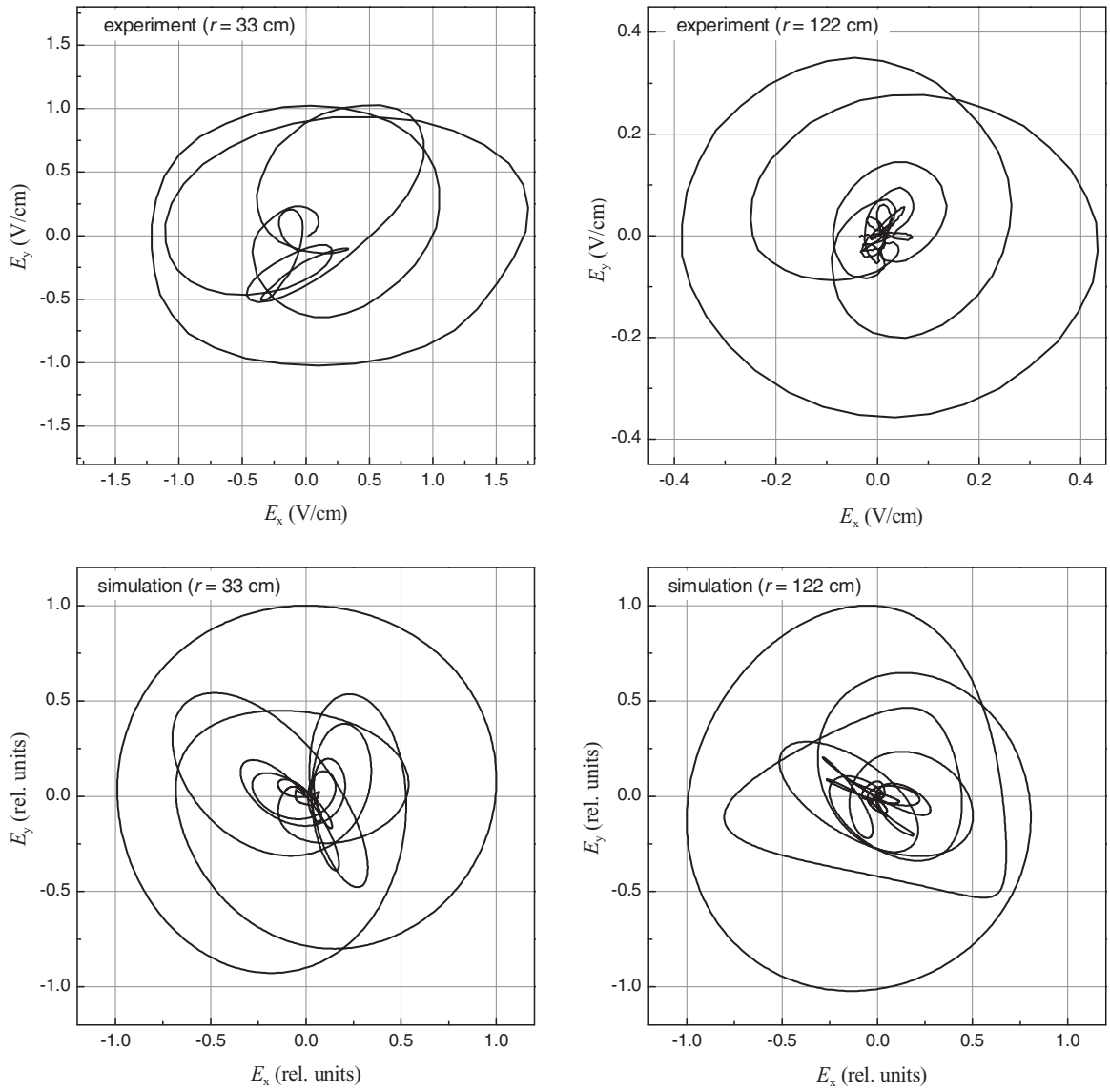

FIG. 9. Simulated and measured hodographs of electric field strength vector at a distance of 33 and 122 cm from the ground plate of helical antenna ($\theta = 0°$).

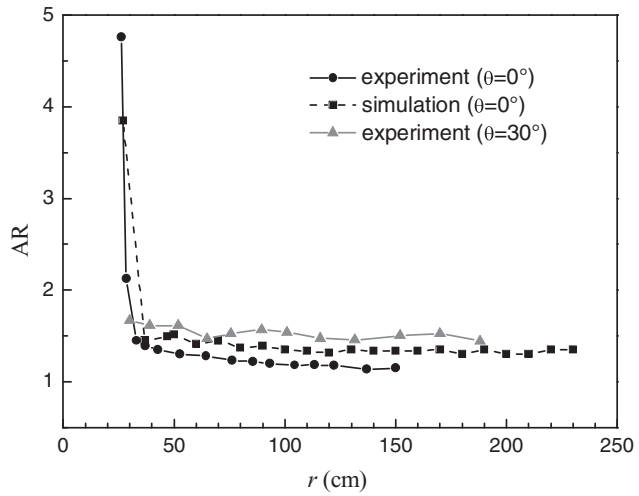

FIG. 10. AR value versus the distance from helical-antenna ground plate ($\theta = 0°$, $\theta = 30°$).

right-hand part of the expression by 10, we can get the estimation of the far-field zone boundary as $r \cong 1.5\lambda$. For the lower frequency band, maximum value of the distance r is 0.66 m. Thus, the far-field zone boundary evaluated by the results of the investigations as $r \cong 1.2$ m has good agreement with the above-mentioned analytical estimations.

The patterns were studied in physical and numerical experiments and measured in two orthogonal planes: X and Y. For each of the chosen planes, θ and φ electric field components were measured. Fig. 11 presents the experimental pattern $E^2_{p\varphi}(\theta)$ by the peak power for the φ-component of the electric field and corresponding simulated pattern for the antenna with $N = 4$. As it is seen, the essential difference between the measured and calculated patterns is observed at large angles ($\theta \geq 30°$). This difference is probably due to the simplified approximation of geometry of the transition line from the coaxial feeder to the helical antenna (Fig. 5).

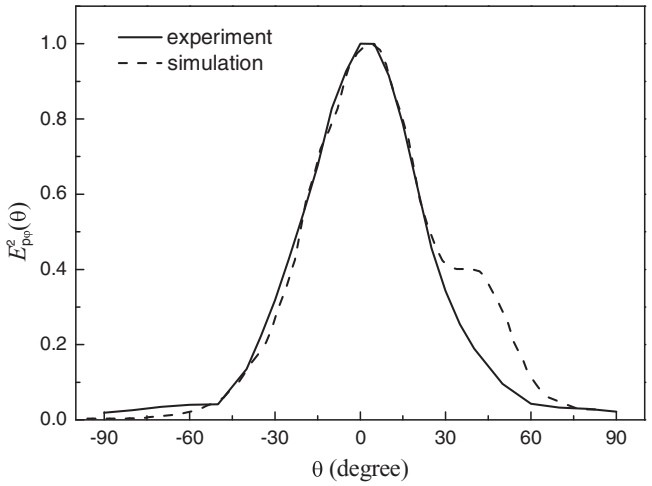

FIG. 11. Measured and simulated normalized patterns by peak power for helical antenna with the number of turns $N = 4$.

The patterns of the helical antennas with the number of turns equal to 3–5 were investigated as well. The measurements have shown that at a small number of turns ($N = 3$–4) the pattern maximum of the helical antenna deviates from the axis at 2°–3°. At $N \geq 5$, the pattern maximum is located near the axis of the helical antenna. The ratio E_p in the forward ($\theta = 0°$) and backward ($\theta = 180°$) directions at the number of the helix turns $N = 3$–5 is approximately equal to 6. Increase of the number of turns results in decrease of the antenna pattern width. Table I presents the data of the antenna patterns at FWHM.

The dielectric container had no essential effect on the pattern of the helical antenna for a variant when $N = 4$. The patterns measured allow determining a directivity parameter of the antenna at the axis D_0.[30] For the antenna with $N = 4$, the value of $D_0 = 13.8$, that is close to the calculated value of $D_0 = 13.5$ obtained by the formula[27]

$$D_0 = 15N\frac{C^2S}{\lambda^3}$$

for the wavelength $\lambda = 26.7$ cm corresponding to the frequency $f = 1.12$ GHz.

The value of AR of the helical antenna radiation was also measured with a TEM-antenna. The receiving antenna had vertical and horizontal positions in the measuring point to record the E_y and E_x components of the electric field. The oscilloscope was triggered by the pulse from the output of an additional antenna which had a changeless position during measurements allowing recording a phase shift between the $E_y(t)$ and $E_x(t)$ pulses with a small error at a high stability of radiation. The measurements have shown that AR varies slightly in the limits of the angle $\theta \leq 20°$ and the AR value reaches 1.2 for the antenna with $N = 4$. In the dielectric container, the values of AR differed insignificantly from the AR values of the antenna radiation field without a container.

TABLE I. FWHM of the peak power pattern.

N	X plane θ-polarization (deg)	X plane φ- polarization (deg)	Y plane θ- polarization (deg)	Y plane φ- polarization (deg)
3	48.5	49.0	51.0	43.0
3.5	48.0	48.0	51.0	41.0
4	43.5	46.0	50.5	39.5
4.5	42.0	44.0	46.5	38.0
5	39.5	40.5	46.0	37.0
5.5	37.5	38	42.0	37.5

V. RADIATION OF HIGH-POWER UWB PULSES

Figure 1 presents an external view of a high-power UWB radiation source. Radiation characteristics of the high-power UWB source were measured in an anechoic chamber. The LeCroy Wave Master 830Zi-A and Tektronix TDS 6604 oscilloscopes were used, respectively, to record radiated pulses and high-voltage pulses at the input of the helical antenna.

A voltage pulse (Fig. 4) from the bipolar voltage pulse generator entered the input of a transmitting helical antenna with $N = 4$. This number of turns was mainly determined by better matching of the antenna and feeder. Recording of radiated pulses was realized by means of the TEM-antenna at a distance $r = 4.6$ m both at the antenna axis ($\theta = 0°$) and at the deviation of radiation direction from the axis to the angle $\theta = \pm 10°$ in a horizontal (X) plane. Fig. 12 presents radiation waveforms for the horizontal and vertical components of the field for $\theta = 0°$. In these measurements, the time shift between $E_y(t)$ and $E_x(t)$ pulses was taken into account as well.

The hodograph is shown in Fig. 13 in the coordinates E_x and E_y corresponding to the horizontal and vertical components of the electric field in the receiving point (at a 4.6 m distance from the radiation center of the helical antenna). The value of AR = 1.3 at the axis of the helical antenna ($\theta = 0°$) remains the same for the points ($\theta = 10°$, $\varphi = 0°$), ($\theta = 10°$, $\varphi = 180°$). The effective potential of radiation rE_p at the axis in the point r = 4.6 m equals to 280 kV. In this case, $k_E = rE_p/U_{g\,max} = 1.4$, that increases essentially the value of $k_E = 0.44$ for the UWB source with a helical antenna having the number of turns $N = 2$.[18]

In case the spectrum of the voltage pulse at the antenna input and VSWR of the antenna are known, one can find the

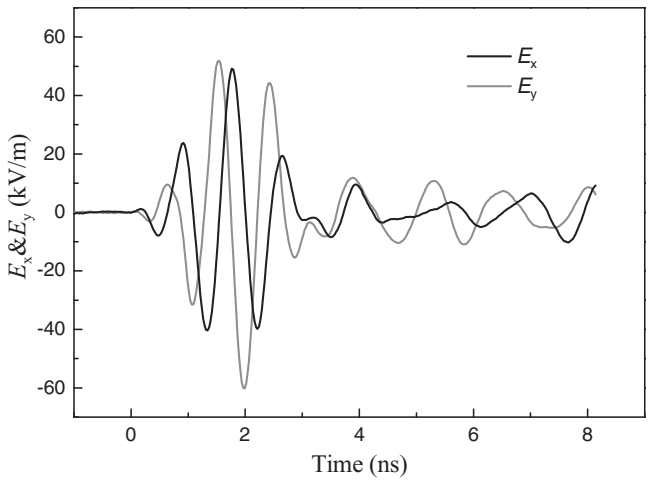

FIG. 12. Radiated pulse waveforms for horizontal and vertical field components ($\theta = 0°$).

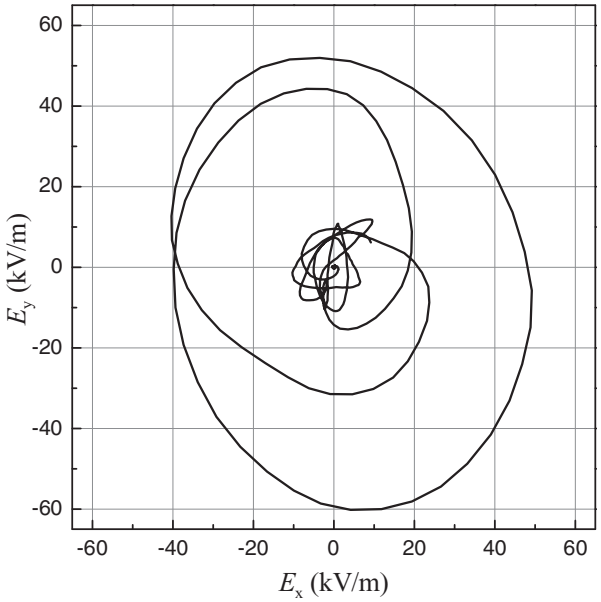

FIG. 13. Hodograph of electric-field vector.

antenna efficiency by the energy k_w. Reflected energy was determined by the ratio:[31]

$$\frac{W_{ref}}{W_g} = \frac{\int U_g^2(f)\left(\frac{K_V(f)-1}{K_V(f)+1}\right)^2 df}{\int U_g^2(f) df},$$

where W_{ref} is the reflected energy, W_g is the generator pulse energy, $U_g(f)$ is the spectrum of the generator voltage pulse, K_V is the VSWR of the antenna in the dielectric case. The reflected energy estimated in this way makes up 0.25 of the generator pulse energy, that corresponds to the energy efficiency of the antenna $k_w = 1 - W_{ref}/W_g = 0.75$. Direct measurements of reflected energy have good agreement with the above-cited.

During an hour of the UWB source operation at a pulse repetition rate of 100 Hz, the change in the chosen points of the amplitude E_p averaged over a hundred pulses was not higher than 15% and the root-mean-square deviation of the amplitude σ during the same one hundred pulses did not exceed 6% (Fig. 14).

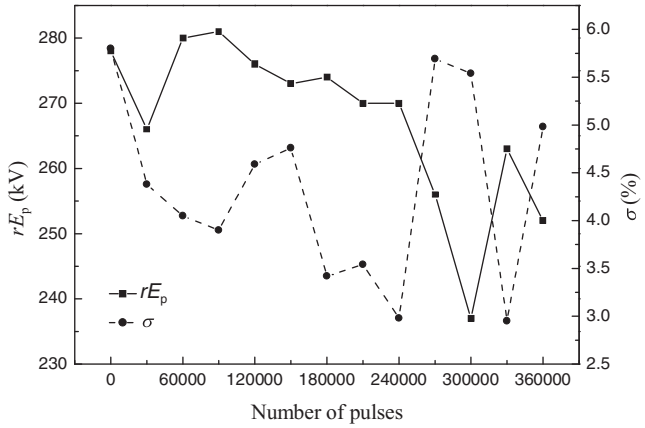

FIG. 14. Effective potential of radiation and its root-mean-square deviation versus the number of pulses.

VI. CONCLUSIONS

A source of high-power ultrawideband radiation with elliptical polarization has been created. The helical antenna with the number of turns $N = 4$ is excited with a high-voltage bipolar pulse. The source operates at a 100 Hz pulse repetition rate. The time of continuous running is 1 h. The energy efficiency of the antenna is 0.75 at the value of the AR of radiation at the axis equal to 1.3. The effective potential of radiation of the source at the voltage amplitudes of the bipolar pulse generator of −175/+200 kV reaches 280 kV.

ACKNOWLEDGMENTS

The authors are grateful to E. V. Balzovsky for his help with the measurements. The authors are also grateful to the Regional Common Use Center of Tomsk Scientific Center SB RAS for the provided LeCroy Wave Master 830Zi-A oscilloscope.

The work was supported by the program of fundamental research of the Presidium of RAS "Basic Problems of Pulsed High-Current Electronics."

[1] D. Nitsch, M. Camp, F. Sabat, J. L. ter Haseborg, and H. Garbe, IEEE Trans. Electromagn. Compat. **46**, 380 (2004).
[2] D. V. Giri, H. Lackner, I. D. Smith, D. W. Morton, C. E. Baum, J. R. Marek, W. D. Prather, and D. W. Scholfield, IEEE Trans. Antennas Propagat. **25**, 318 (1997).
[3] F. Sabat, D. Nitsch, M. Jung, and T. H. G. G. Weise, IEEE Trans. Antennas Propagat. **30**, 1722 (2002).
[4] A. Pokryvailo, Y. Yankelevich, and M. Shapiro, IEEE Trans. Plasma Sci. **32**, 1909 (2004).
[5] Y. S. Jin, S. W. Lim, C. H. Cho, J. S. Kim, Y. B. Kim, S. H. Lee, and Y. Roh, Rev. Sci. Instrum. **83**, 044704 (2012).
[6] Yu. A. Andreev, V. P. Gubanov, A. M. Efremov, V. I. Koshelev, S. D. Korovin, B. M. Kovalchuk, V. V. Kremnev, V. V. Plisko, A. S. Stepchenko, and K. N. Sukhushin, Laser Part. Beams **21**, 211 (2003).
[7] V. I. Koshelev, Yu. A. Andreev, A. M. Efremov, B. M. Kovalchuk, V. V. Plisko, K. N. Sukhushin, and S. Liu, J. Energy Power Eng. **6**, 771 (2012).
[8] I. V. Romanchenko, V. V. Rostov, V. P. Gubanov, A. S. Stepchenko, A. N. Gunin, and I. K. Kurkan, Rev. Sci. Instrum. **83**, 074705 (2012).
[9] Yu. A. Andreev, V. I. Koshelev, I. V. Romanchenko, V. V. Rostov, and K. N. Sukhushin, J. Commun. Technol. Electron. **58**, 297 (2013).
[10] V. P. Gubanov, A. M. Efremov, V. I. Koshelev, B. M. Koval'chuk, S. D. Korovin, V. V. Plisko, A. S. Stepchenko and K. N. Sukhushin, Instrum. Exp. Tech. **48**, 312 (2005).
[11] A. M. Efremov, V. I. Koshelev, B. M. Kovalchuk, V. V. Plisko, and K. N. Sukhushin, J. Commun. Technol. Electron. **52**, 756 (2007).
[12] A. M. Efremov, V. I. Koshelev, B. M. Kovalchuk, V. V. Plisko, and K. N. Sukhushin, Instrum. Exp. Tech. **54**, 70 (2011).
[13] Yu. A. Andreev, A. M. Efremov, V. I. Koshelev, B. M. Kovalchuk, V. V. Plisko, and K. N. Sukhushin, Instrum. Exp. Tech. **54**, 794 (2011).
[14] Yu. A. Andreev, A. M. Efremov, V. I. Koshelev, B. M. Kovalchuk, V. V. Plisko, and K. N. Sukhushin, J. Commun. Technol. Electron. **56**, 1429 (2011).
[15] A. M. Efremov, V. I. Koshelev, B. M. Kovalchuk, and V. V. Plisko, Instrum. Exp. Tech. **56**, 302 (2013).
[16] J. R. Mayes, M. G. Mayes, W. C. Nunnally, and C. W. Hatfield, in *Proceedings of the 17th IEEE Pulsed Power Conference* (IEEE, 2009), Vol. 1, p. 484.
[17] D. Morton, J. Banister, T. DaSilva, J. Livine, T. Naff, I. Smith, H. Sze, T. Warren, D. V. Giri, C. Mora, J. Pavlinko, J. Schleher, and C. E. Baum, in *Proceedings of the IEEE International Power Modul. High Voltage Conference* (IEEE, 2010), Vol. 1, p. 186.
[18] Y. Wang, D. Chen, Z. Zhang, S. Cao, D. Lii, and C. Liu, Rev. Sci. Instrum. **84**, 094705 (2013).

[19]M. Yu. Zorkaltseva, V. I. Koshelev, and A. A. Petkun, Russ. Phys. J. **56**(10/3), 149 (2013).
[20]J. D. Kraus, Proc. IRE **36**, 1236 (1948).
[21]H. E. King and J. L. Wong, IEEE Trans. Antennas Propagat. **28**, 291 (1980).
[22]M. E. Dunham, M. Light, and D. N. Holden, IEEE Trans. Antennas Propagat. **43**, 1017 (1995).
[23]D. V. Giri, F. M. Tesche, M. D. Abdalla, M. C. Skipper, and M. Nyffeler, IEEE Trans. Plasma Sci. **38**, 1411 (2010).
[24]S. Sander and D. K. Cheng, IRE Nat. Conv. Rec. **6**, 152 (1958).
[25]N. Barbano, IRE Wescon Conv. Rec. **4**, 123 (1960).
[26]A. R. Djordjevic, A. G. Zajic, M. M. Ilic, and C. L. Stuber, IEEE Trans. Antennas Propagat. Mag. **48**, 107 (2006).
[27]C. A. Balanis, *Antenna Theory: Analysis and Design*, 2nd ed. (Wiley, New York, 1997).
[28]See http://www.qsl.net/4nec2/ for information about 4NEC2 code.
[29]E. V. Balzovskii, Yu. I. Buyanov, and V. I. Koshelev, J. Commun. Technol. Electron. **55**, 172 (2010).
[30]Yu. A. Andreev, Yu. I. Buyanov, and V. I. Koshelev, J. Commun. Technol. Electron. **50**, 535 (2005).
[31]V. I. Koshelev and V. V. Plisko, Russ. Phys. J. **56**(10/3), 134 (2013).